

Two-Dimensional l_1 -Norm Minimization in SAR Image Reconstruction

A. Lazarov, D. Minchev

*Faculty of Computer Science and Engineering, Burgas Free University, Burgas, Bulgaria
Emails: lazarov@bfu.bg; mitko@bfu.bg*

Abstract: *A nonconventional image algorithm, based on compressed sensing and l_1 -norm minimization in Synthetic Aperture Radar (SAR) application is discussed. A discrete model of the earth surface relief and mathematical modeling of SAR signal formation are analytically described. Sparse decomposition in Fourier basis to solve the SAR image reconstruction problem is discussed. In contrast to the classical one-dimensional definition of l_1 -norm minimization in SAR image reconstruction, applied to an image vector, the present work proposes a two-dimensional definition of l_1 -norm minimization to the image. To verify the correctness of the algorithm, results of numerical experiments are presented.*

Keywords: *SAR image reconstruction, compressed sensing, 2D l_1 -norm minimization.*

1. Introduction

Synthetic Aperture Radar (SAR) is a powerful instrument for monitoring the relief of the earth surface, by illuminating electromagnetic pulses and coherent registration of the backscattered radiation [1-3]. The resulting images are registered in a two-dimensional coordinate system: slant range coordinate or coordinate of the time delay and azimuth or cross range coordinate. High resolution on the slant range direction is achieved by wide bandwidth emitted pulses, while high resolution on the cross range is achieved by coherent summation of the reflected signals during the aperture synthesis.

Conventional nonparametric SAR imaging algorithms are correlation based on the theory of the matched filter. Their resolution properties are limited by the bandwidth of the transmitted signal and the synthetic aperture length, known as Nyquist constraints. To surmount these circumstances in case of sparse image

decomposition, a new computational technique, called Compressed Sensing (CS) is applied. It consists of minimizing an objective function which includes a square Euclidian term combined with a sparseness-inducing l_1 regularization term [4].

Much attention has been paid to l_1 -norm optimization based methods for sparse image reconstruction (e.g., basis pursuit denoising, wavelet-based deconvolution and compressed sensing) and feature selection (e.g., Least Absolute Shrinkage and Selection Operator (LASSO) algorithm in signal and image processing, statistics, and related fields. These problems can be considered as l_1 -regularized Least-Squares Programs (LSPs), which can be reformulated as convex quadratic programs [5], and then solved by several standard methods, such as interior-point methods [6]. Sparse image reconstruction by application of l_1 -norm minimization is used in the reconstruction of a finite-dimensional sparse vector, based on its linear measurements of a dimension, smaller than the size of the unknown sparse vector [7, 8].

A data acquisition system for wideband synthetic aperture imaging and reconstruction of the sparse signals from a small set of non-adaptive linear measurements, based on CS by exploiting the sparseness of point-like targets in the image space and by solving a convex l_1 -norm minimization problem, is presented in [9]. CS method for 3D buried point-like targets imaging for continuous-wave ground penetrating radar is discussed in [10, 11]. It is shown that the image of the sparse targets can be reconstructed by solving a constrained convex optimization problem based on l_1 -norm minimization with only a small number of the data from randomly selected frequency samples and antenna scan positions, which will reduce the data collecting time. A compressive noise radar imaging algorithm, using l_1 -norm based sparsity constraints and convex optimization is discussed in [12].

Based on the assumption that SAR imaging algorithms can reconstruct the target scene with a reduced number of collected samples by applying CS approach, a distributed compressed sensing method into a long-track interferometric SAR is introduced, achieving good performance for even fewer samples than that based on compressed sensing [13].

A random-frequency SAR imaging CS scheme is proposed in [14]. It is proved that if the targets are sparse or compressible, it is sufficient to transmit only a small number of random frequencies to reconstruct the image of the targets.

A SAR high resolution CS imaging algorithm in range and azimuth directions is proposed in [15]. A 3D imaging CS algorithm for a linear array SAR and sparse observed surface of the dominating scatterers is developed in [16]. A high resolution CS imaging method, based on l_1 -norm minimization for SAR sparse targets reconstruction and compressed sensing l_0 minimization 2D algorithm for passive ISAR with DVB-T signal are discussed in [17, 18]. In contrast to the aforementioned l_1 -norm minimization, CS algorithms, where the sparse image and signal are presented as a vector, in the present work the sparse image and SAR signal are presented as 2D matrices that require respective mathematical description of the l_1 -norm minimization CS imaging algorithm.

The main goal of this work is on the basis of the geometrical model of the earth surface and mathematical model of SAR signals to develop a SAR image

reconstruction algorithm based on 2D SAR signal decomposition and l_1 -norm minimization of the image sparse feature. The rest of the paper is organized as follows. In Section 2 SAR geometry and kinematics are described. In Section 3 a model of SAR signal, reflected from the observed surface is derived. In Section 4 a sparse decomposition approach to solve the image reconstruction problem is presented. In Section 5 an image reconstruction algorithm, based on sparse SAR signal decomposition and l_1 - norm minimization is discussed. In Section 6 the results of a numerical experiment are presented. In Section 7 some conclusions are made.

2. SAR geometry and kinematics

SAR geometry is defined in the coordinate system $Oxyz$ (Fig. 1). The radar transceiver system is mounted on a spacecraft platform. The movement of SAR satellite is described by the following vector equation

$$(1) \quad \mathbf{R}(p) = \mathbf{R}_0 + \mathbf{V}T_p \cdot p,$$

where: \mathbf{V} is the satellite velocity vector; T_p is the pulse repetition period; $p = \overline{0, N-1}$ is the index of the emitted pulse; N is the full number of emitted pulses during aperture synthesis; $\mathbf{R}_0 = \mathbf{R}(p)$ is the distance vector from the origin of the coordinate system to the satellite at moment $p = 0$.

The vector equation (1) is projected onto the coordinate axes Ox , Oy and Oz , i.e.,

$$(2) \quad \begin{aligned} x(p) &= x_0 - V_x T_p \cdot p, \\ y(p) &= y_0 - V_y T_p \cdot p, \\ z(p) &= z_0 - V_z T_p \cdot p, \end{aligned}$$

where: $x(p)$, $y(p)$ and $z(p)$ are the current satellite coordinates at moment p ; $x_0 = x(0)$, $y_0 = y(0)$ and $z_0 = z(0)$ are the satellite coordinates at moment $p = 0$; $V_x = V \cos \alpha$, $V_y = V \cos \beta$ and $V_z = V \cos \delta$ are coordinates of the velocity vector; α , β and γ are the guiding angles of the velocity vector. The surface of observation is depicted in a coordinate system $Oxyz$. The position of the ijk -th point scatterer on the surface is defined by a distance vector \mathbf{R}_{ijk} with coordinates: $x_{ijk} = (i \cdot \Delta x)$, $y_{ijk} = (j \cdot \Delta y)$ and $z_{ijk} = (k \cdot \Delta z)$. The model of the surface can be analytically described as function $k = k(i, j)$, i.e.,

$$(3) \quad k = k(i, j) = 3(1-i)^2 \exp[-i^2 - (j+1)^2] - 10 \left(\frac{i}{5} - i^3 - j^5 \right) \exp(i^2 - j^2) - \frac{1}{3} \exp[-(i+1)^2 - j^2].$$

During the process of observation the distance vector $\mathbf{R}_{ijk}(p)$ from SAR, located on the satellite with a distance vector $\mathbf{R}(p)$ to the ijk -th point scatterer on

the surface, defined by the distance vector \mathbf{R}_{ijk} can be expressed by the vector equation:

$$(4) \quad \mathbf{R}_{ijk}(p) = \mathbf{R}(p) - \mathbf{R}_{ijk}.$$

The main geometrical characteristic of SAR signal is the module of the distance vector $R_{ijk}(p)$, defined by the expression

$$(5) \quad R_{ijk}(p) = \sqrt{[x_{ijk}(p)]^2 + [y_{ijk}(p)]^2 + [z_{ijk}(p)]^2},$$

where

$$(6) \quad \begin{aligned} x_{ijk}(p) &= x(p) - x_{ijk}, \\ y_{ijk}(p) &= y(p) - y_{ijk}, \\ z_{ijk}(p) &= z(p) - z_{ijk}, \end{aligned}$$

are the current coordinates of the ijk -th point scatterer with respect to the position of the SAR carrier (Fig. 1).

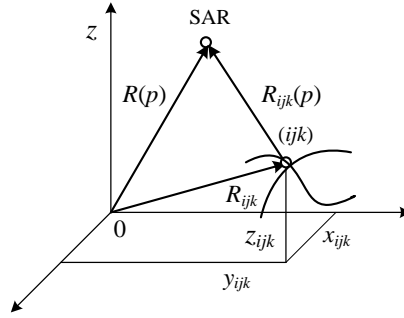


Fig. 1. SAR geometry and kinematics

3. SAR modeling of SAR signal, reflected from the observed surface

Assume that the SAR transmitter emits series of LFM electromagnetic pulses, analytically described by the expression

$$(7) \quad S(t) = \sum_{p=0}^{N-1} \text{rect} \frac{t - pT_p}{T} \exp[-j(\omega t + bt^2)],$$

where:

$$\text{rect} \frac{t - pT_p}{T} = \begin{cases} 1 & \text{if } 0 \leq \frac{t - pT_p}{T} < 1, \\ 0 & \text{otherwise;} \end{cases}$$

$\omega = 2\pi \frac{c}{\lambda}$ is the angular frequency; $p = \overline{0, N-1}$ is the current number of the

emitted LFM pulse; $c = 3.10^8$ m/s is the speed of the light; $b = \frac{\pi \Delta F}{T_k}$ is the LFM

index; ΔF is the bandwidth of the emitted pulse that defines the range resolution; $\Delta R = c / 2\Delta F$, T is the time duration of LFM pulse.

The deterministic component of SAR signal, reflected from the ijk -th point scatterer for any particular p can be written as

$$(8) \quad S_{ijk}(t) = a_{ijk} \mathbf{rect} \frac{t - t_{ijk}}{T} \cdot \exp \left\{ -j \left[\omega(t - t_{ijk}) + b(t - t_{ijk})^2 \right] \right\},$$

where:

$$(9) \quad \mathbf{rect} \frac{t - t_{ijk}(p)}{T_k} = \begin{cases} 1 & \text{if } \frac{t - t_{ijk}(p)}{T_k} \leq 1, \\ 0 & \text{otherwise;} \end{cases}$$

a_{ijk} is the intensity of the ijk -th point scatterer; $t_{ijk}(p) = \frac{2R_{ijk}(p)}{c}$ is the time delay of the signal reflected by the ijk -th point scatterer.

The deterministic component of the SAR signal, reflected from the entire surface can be regarded as a geometrical sum of the signals reflected by all point scatterers on the surface of observation and can be expressed as follows:

$$(10) \quad S(t) = \sum_{ijk} a_{ijk} \mathbf{rect} \frac{t - t_{ijk}(p)}{T_k} \cdot \exp \left\{ -j \left[\omega(t - t_{ijk}(p)) + b(t - t_{ijk}(p))^2 \right] \right\}.$$

Here $t = t_{ijk \min}(p) + (k-1)\Delta T$ are the time parameter, measured on the range direction for each p ; $k = \overline{0, K-1}$ is the range sample (fast time) index; ΔT is the timewidth of LFM sample; K is the full number of range samples.

Two-dimensional Taylor expansion of $\omega(t - t_{ijk}(p)) + b(t - t_{ijk}(p))^2$ in the vicinity of the unknown discrete coordinates \hat{p} and \hat{k} of the ijk -th point scatterers yields

$$(11) \quad \tilde{S}(p, k) = \sum_{\hat{p}, \hat{k}} a(\hat{p}, \hat{k}) \mathbf{exp} \left\{ -j \left[2\pi \cdot \frac{p \cdot \hat{p}}{\hat{N}} + 2\pi \cdot \frac{k \cdot \hat{k}}{\hat{K}} + \Phi(p, k) \right] \right\},$$

where: $a(\hat{p}, \hat{k})$ is the 2D image function; $\Phi(p, k)$ is the phase term of higher order; $\hat{p} = \overline{0, \hat{N}-1}$; $\hat{k} = \overline{0, \hat{K}-1}$; \hat{N} and \hat{K} denote the full number of image points coordinates on the cross range (azimuth) and range directions, respectively.

Assume that $\Phi(p, k) = 0$, then (11) can be rewritten in a matrix form

$$(12) \quad \mathbf{S} = \mathbf{P} \cdot \mathbf{A} \cdot \mathbf{K}^T,$$

where: $\mathbf{S}(N \times K)$ is the complex signal matrix; $\mathbf{P}(N \times \hat{N}) = \left[\exp \left(-j \frac{2\pi p \cdot \hat{p}}{\hat{N}} \right) \right]$ is

the Discrete Fourier Transform (DFT) matrix (cross-range matrix-dictionary);

$\mathbf{K}(K \times \hat{K}) = \left[\exp \left(-j \frac{2\pi k \cdot \hat{k}}{\hat{K}} \right) \right]$ is the DFT matrix (range matrix-dictionary);

$\mathbf{A}(\hat{N} \times \hat{K})$ is the image matrix. In SAR application the dimension of the reconstructed image is equal to the dimension of the registered signal, i.e., $\hat{N} = N$ and $\hat{K} = K$.

4. Sparse decomposition approach to solve the image reconstruction problem

Expression (12) denotes 2D discrete Fourier decomposition of the signal in a matrix form. It means that the two-dimensional signal $\mathbf{S} \in \mathbf{R}^{N \times K}$ is a linear combination of the columns of matrices \mathbf{P} and \mathbf{K} . In case $N = \hat{N}$ (complete measurement), the decomposition (12) is unique, it means that there exists a unique sparsest solution for \mathbf{A} . Defining the compressed sensing measured matrix,

$$\mathbf{X} = \Phi_p \cdot \mathbf{S} \cdot \Phi_k^T + \mathbf{W} \in \mathbf{R}^{N' \times K'} \quad \text{or} \quad \mathbf{X} = \Phi_p \cdot \mathbf{P} \cdot \mathbf{A} \cdot \mathbf{K}^T \cdot \Phi_k^T + \mathbf{W} \in \mathbf{R}^{N' \times K'}$$

over the redundant Fourier dictionaries $\hat{\mathbf{P}} = \Phi_p \cdot \mathbf{P} \in \mathbf{R}^{N' \times \hat{N}}$ and $\hat{\mathbf{K}} = \Phi_k \cdot \mathbf{K} \in \mathbf{R}^{K' \times \hat{K}}$, where $\Phi_p (N' \times N)$ and $\Phi_k (K' \times K)$ are pseudo identity sensing matrices, \mathbf{W} is the white Gaussian noise matrix. In the over-complete case $N' < \hat{N}$ and $K' < \hat{K}$, matrix \mathbf{X} does not have unique decomposition. The reconstruction of the image matrix \mathbf{A} can be implemented by solving a convex optimization constrained problem [18]

$$(13) \quad \min \|\mathbf{A}\|_1 \quad \text{subject to} \quad \|\mathbf{X} - \hat{\mathbf{P}} \cdot \mathbf{A} \cdot \hat{\mathbf{K}}^T\|_F^2 \leq \varepsilon,$$

$$(14) \quad \min \|\mathbf{X} - \hat{\mathbf{P}} \cdot \mathbf{A} \cdot \hat{\mathbf{K}}^T\|_F^2 \leq \varepsilon \quad \text{subject to} \quad \|\mathbf{A}\|_1 < t,$$

where $\|\mathbf{A}\|_1 = (\mathbf{1}_{\hat{N}}^T \cdot \mathbf{A})_{\text{mcs}}$ is the l_1 -norm of the matrix \mathbf{A} .

The l_1 -norm of the image matrix $\|\mathbf{A}\|_1$ can be expressed as a maximum absolute

column sum of point scatterers intensities, i.e., $(\mathbf{1}_{\hat{N}}^T \cdot \mathbf{A})_{\text{mcs}} = \max_{\hat{k}=0, \hat{K}-1} \left(\sum_{\hat{p}=0}^{\hat{N}-1} |a_{\hat{p}\hat{k}}| \right)$, where

$a_{\hat{p}\hat{k}}$ is the element of the image matrix \mathbf{A} , $\mathbf{1}_{\hat{N}}$ is the vector of \hat{N} ones, ε and t are small constants, $\|\mathbf{X} - \hat{\mathbf{P}} \cdot \mathbf{A} \cdot \hat{\mathbf{K}}^T\|_F^2$ denotes the square of the Frobenius norm that can be presented as

$$(15) \quad \|\mathbf{X} - \hat{\mathbf{P}} \cdot \mathbf{A} \cdot \hat{\mathbf{K}}^T\|_F^2 = \mathbf{1}_{N'}^T \cdot \left[(\mathbf{X} - \hat{\mathbf{P}} \cdot \mathbf{A} \cdot \hat{\mathbf{K}}^T)^T (\mathbf{X} - \hat{\mathbf{P}} \cdot \mathbf{A} \cdot \hat{\mathbf{K}}^T) \right] \cdot \mathbf{1}_{K'},$$

$$(16) \quad \|\mathbf{X} - \hat{\mathbf{P}} \cdot \mathbf{A} \cdot \hat{\mathbf{K}}^T\|_F^2 = \mathbf{1}_{N'}^T \cdot \left[(\mathbf{X}^T - \hat{\mathbf{K}} \cdot \mathbf{A}^T \cdot \hat{\mathbf{P}}^T) (\mathbf{X} - \hat{\mathbf{P}} \cdot \mathbf{A} \cdot \hat{\mathbf{K}}^T) \right] \cdot \mathbf{1}_{K'},$$

$$= \mathbf{1}_{N'}^T \cdot \left(\mathbf{X}^T \mathbf{X} - 2 \mathbf{X}^T \cdot \hat{\mathbf{P}} \cdot \mathbf{A} \cdot \hat{\mathbf{K}}^T + \hat{\mathbf{K}} \cdot \mathbf{A}^T \cdot \hat{\mathbf{P}}^T \cdot \hat{\mathbf{P}} \cdot \mathbf{A} \cdot \hat{\mathbf{K}}^T \right) \cdot \mathbf{1}_{K'}^T,$$

where $\mathbf{1}_{K'}$ and $\mathbf{1}_{N'}$ are vectors of K' and N' ones, respectively.

Summarizing (13) and (14) the image matrix \mathbf{A} can be extracted by the following unconstrained optimization scalar object function

$$(17) \quad F(\mathbf{A}) = \min \left(\frac{1}{2} \|\mathbf{X} - \hat{\mathbf{P}} \cdot \mathbf{A} \cdot \hat{\mathbf{K}}^T\|_F^2 + \tau \|\mathbf{A}\|_1 \right),$$

where τ is the nonnegative weighing parameter.

Disclose the square of the Frobenius norm and l_1 -norm in a matrix form, then

$$(18) F(\mathbf{A}) = \min \left[\frac{1}{2} \mathbf{1}_{N'}^T (\mathbf{X}^T \mathbf{X} - 2\mathbf{X}^T \hat{\mathbf{P}} \mathbf{A} \hat{\mathbf{K}}^T + \hat{\mathbf{K}} \mathbf{A}^T \hat{\mathbf{P}}^T \hat{\mathbf{P}} \mathbf{A} \hat{\mathbf{K}}^T) \mathbf{1}_{K'}^T + \tau \cdot (\mathbf{1}_{\hat{N}}^T \mathbf{A})_{\text{mcs}} \right],$$

where **mcs** denotes maximum column sum.

As the measured matrix \mathbf{X} consists of constant entries, the matrix multiplication $\mathbf{X}^T \mathbf{X}$ does not influence on the unconstrained optimization problem and can be removed, then

$$(19) F(\mathbf{A}) = \min \left(\frac{1}{2} \mathbf{1}_{N'}^T (-2\mathbf{X}^T \hat{\mathbf{P}} \mathbf{A} \hat{\mathbf{K}}^T + \hat{\mathbf{K}} \mathbf{A}^T \hat{\mathbf{P}}^T \hat{\mathbf{P}} \mathbf{A} \hat{\mathbf{K}}^T) \mathbf{1}_{K'}^T + \tau \cdot (\mathbf{1}_{\hat{N}}^T \mathbf{A})_{\text{mcs}} \right).$$

The final expression of the optimization objective function obtains the form

$$(20) F(\mathbf{A}) = \min \left(\frac{1}{2} \mathbf{1}_{N'}^T (-2\mathbf{X}^T + \hat{\mathbf{K}} \mathbf{A}^T \hat{\mathbf{P}}^T) (\hat{\mathbf{P}} \mathbf{A} \hat{\mathbf{K}}^T) \mathbf{1}_{K'}^T + \tau \cdot (\mathbf{1}_{\hat{N}}^T \mathbf{A})_{\text{mcs}} \right).$$

In order to create a reconstruction algorithm the first derivative of the scalar objective function has to be extracted, it means to find out first order derivative of the scalar $F(\mathbf{A})$ in respect of elements of the image matrix \mathbf{A} . The result is known as a gradient matrix

$$(21) \quad \nabla F(\mathbf{A}) = \frac{\partial F(\mathbf{A})}{\partial \mathbf{A}} = \sum_{\hat{k}=0}^{\hat{K}-1} \sum_{\hat{p}=0}^{\hat{N}-1} \mathbf{E}_{\hat{p}, \hat{k}} \frac{\partial F(\mathbf{A})}{\partial a_{\hat{p}, \hat{k}}},$$

where $\mathbf{E}_{\hat{p}, \hat{k}}$ denotes the elementary matrix of order $(\hat{N} \times \hat{K})$. The elementary matrix has all zero entries except for the \hat{p}, \hat{k} entry, which is one.

5. Image Reconstruction Algorithm Based on Sparse Decomposition

Calculate the initial estimate of the image matrix $\mathbf{A} = \mathbf{A}^0$ based on the expression

$$(22) \quad \begin{aligned} & (\hat{\mathbf{P}} \mathbf{A} \hat{\mathbf{K}}^T - \mathbf{X})^T \approx \mathbf{0}, \text{ i.e.,} \\ & \mathbf{A}^0 = \hat{\mathbf{P}}^* \mathbf{X} (\hat{\mathbf{K}}^*)^T, \end{aligned}$$

where $\hat{\mathbf{P}}^* = \left[\exp \left(j \frac{2\pi \hat{p} \cdot p}{\hat{N}} \right) \right]$ is the cross range inverse DFT matrix,

$\hat{\mathbf{K}}^* = \left[\exp \left(j \frac{2\pi \hat{k} \cdot k}{\hat{K}} \right) \right]$ is the range inverse DFT matrices, where $p = \overline{0, N'-1}$, $k = \overline{0, K'-1}$.

Minimization l_1 -norm algorithm

Step 1. On each iteration step define a gradient matrix $\mathbf{G}(\hat{N} \times \hat{K})$ with elements equal to elements of $\nabla F(\mathbf{A}^k)$ and define as $\mathbf{G} = \mathbf{G}(\nabla F(\mathbf{A}^k))$ if $\mathbf{A}^k > 0$, or $\nabla F(\mathbf{A}^k) < 0$, otherwise $\mathbf{G}(\nabla F(\mathbf{A}^k))$ equal to $\mathbf{0}$ matrix [4].

Let $k = 0$.

Step 2. Define iteratively an initial value of the Hessian parameter α^0 as an argument minimizing the objective function

$$(23) \quad \alpha^0 = \underset{\alpha}{\operatorname{argmin}} F(\mathbf{A}^0 - \alpha.G(\nabla F(\mathbf{A}^0))).$$

Start search procedure with an arbitrary value α , for example $\alpha = 1$, and then increase α with 0.2. If the scalar $F(\mathbf{A}^0 - \alpha.G(\nabla F(\mathbf{A}^0)))$ decreases then continue with increasing α with 0.1 until global minimum of scalar objective function. If the scalar $F(\mathbf{A}^0 - \alpha.G(\nabla F(\mathbf{A}^0)))$ increases then decrease α with 0.1 until global minimum of $F(\mathbf{A}^0 - \alpha.G(\nabla F(\mathbf{A}^0)))$.

Step 3. Define the decreasing matrix $\Delta^0 = (\mathbf{A}^0 - \alpha^0.G(\nabla F(\mathbf{A}^0)))_+ - \mathbf{A}^0$, where $(\dots)_+$ denotes a positive-part operator, for example

$$(r)_+ = \max\{0, r\} = \begin{cases} r & \text{if } r > 0, \\ 0 & \text{if } r < 0. \end{cases}$$

Step 4. Define iteratively a new image matrix: $\mathbf{A}^1 = \mathbf{A}^0 + \lambda^0.\Delta^0$ by minimizing the scalar object function $F(\mathbf{A}^0 + \lambda^0.\Delta^0)$ for $\lambda^0 \in [0, 1]$.

Let $k = k$.

Step 5. Define a scalar Hessian parameter of proportionality

$$\alpha^k \approx \frac{\mathbf{A}^k - \mathbf{A}^{k-1}}{\nabla F(\mathbf{A}^k) - \nabla F(\mathbf{A}^{k-1})}.$$

Step 6. Define the decreasing matrix $\Delta^k = (\mathbf{A}^k - \alpha^k.G(\nabla F(\mathbf{A}^k)))_+ - \mathbf{A}^k$.

Step 7. Define iteratively a new image matrix: $\mathbf{A}^{k+1} = \mathbf{A}^k + \lambda^k.\Delta^k$ by minimizing the objective function: $F(\mathbf{A}^k + \lambda^k.\Delta^k)$ for $\lambda^k \in [0, 1]$.

Step 8. Terminate the calculation in case the object function $F(\mathbf{A}^{k+1})$ falls into a global minimum otherwise go to point 5.

Parameter τ is defined by applying the approach, suggested in [19], i.e.,

$$(24) \quad \tau = 0.1 \left\| \hat{\mathbf{P}}^*.\mathbf{X}.\hat{\mathbf{K}}^{*T} \right\|_{\infty},$$

where $\left\| \hat{\mathbf{P}}^*.\mathbf{X}.\hat{\mathbf{K}}^{*T} \right\|_{\infty}$ means the maximum absolute row sum of the matrix $\hat{\mathbf{P}}^*.\mathbf{X}.\hat{\mathbf{K}}^{*T}$ which is the first guest of the image matrix \mathbf{A}^0 (22), i.e.,

$$(25) \quad \left\| \mathbf{A}^0 \right\|_{\infty} = \max_{\hat{p}=0, \hat{N}-1} \left(\sum_{\hat{k}=0}^{\hat{K}-1} |a_{\hat{p}\hat{k}}| \right).$$

6. Numerical experiment

Consider SAR scenario with the following parameters. Initial coordinates of the SAR carrier $x_0 = 10^4$ m, $y_0 = 10^4$ m, $z_0 = 8.10^5$ m; vector velocity $V = 10^3$ m/s; guiding angles $\alpha = \pi/4$, $\beta = \pi/4$, $\gamma = 0$. SAR parameters: carrier frequency $f = 10^{10}$ Hz; frequency bandwidth $\Delta F = 2.5.10^7$ Hz; pulse repetition period $2.5.10^{-3}$ s; LFM pulse width $2.5.10^{-6}$ s; number of emitted pulses $N_p = 512$; number of range samples $K = 512$. The geometry of the surface is calculated by the Expression (3) with indices $i = \overline{1, 64}$, $j = \overline{1, 64}$ and displacement between the point scatterers: $\Delta x = \Delta y = \Delta z = 4$ m.

The SAR complex signal matrix \mathbf{S} , calculated by (10) is presented in Fig. 2a (amplitude) and Fig. 2b (phase). The image of the surface extracted from the full size complex signal matrix \mathbf{S} is presented in Fig. 2c.

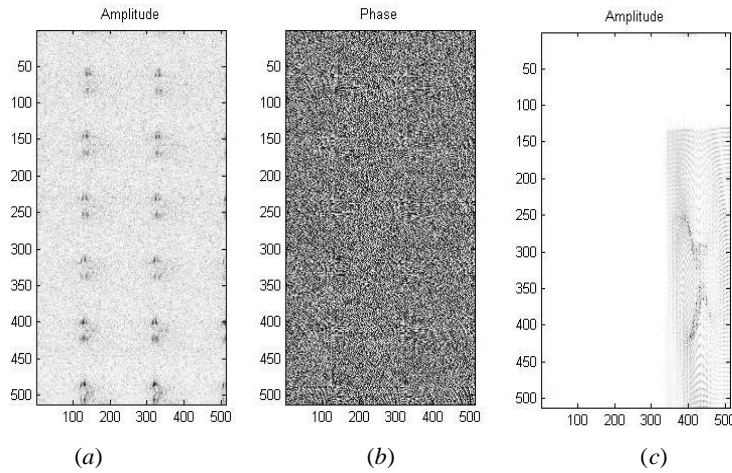


Fig. 2. Full size complex signal matrix \mathbf{S} : Amplitude (a) and phase (b); the image of the surface extracted from matrix \mathbf{S} (c)

The compressed sensing measured complex matrix \mathbf{X} , obtained by multiplication of the original matrix \mathbf{S} with the pseudo identity sensing matrices $\Phi_p (128 \times 512)$ and $\Phi_k (128 \times 512)$, is presented in Fig. 3a (amplitude) and Fig. 3b (phase). The final image is extracted from the compressed sensing matrix \mathbf{X} by applying l_1 -norm minimization algorithm over the image matrix \mathbf{A}^0 (Fig. 3c). The algorithm converges into a global minimum after 12-15 steps, depending on the size of the step in calculation of the Hessian parameter α^0 and determination of a new image matrix by minimizing the object function. It is interesting to note that despite the surface matrix in the plane Oxy has dimensions 64×64 , the SAR image in the plane of observation (p, k) has dimensions 512×512 .

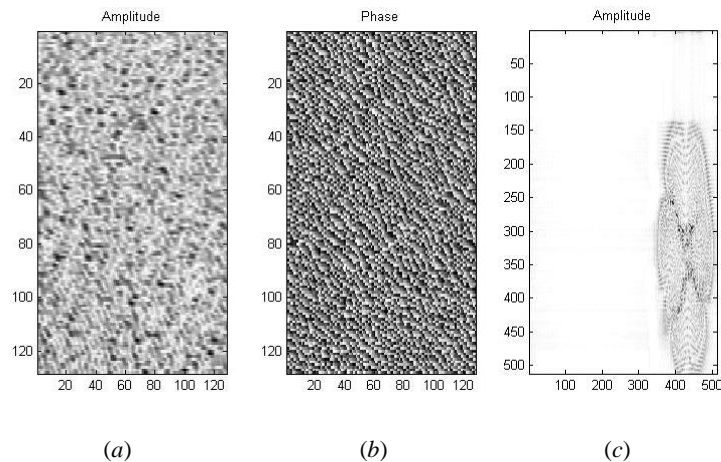


Fig. 3. Compressed sensing measured matrix \mathbf{X} : Amplitude (a) and phase (b); the image of the surface calculated by a compressed sensing matrix \mathbf{X} (c)

7. Conclusion

In this paper a nonconventional image reconstruction algorithm, based on compressed sensing and l_1 -norm minimization in SAR application has been developed. A discrete model of the earth surface relief and the mathematical modelling of SAR signal formation have been analytically described. A sparse decomposition in Fourier basis to solve SAR image reconstruction problem has been discussed. In contrast to the classical one-dimensional definition of l_1 -norm minimization in SAR image reconstruction, applied to an image vector, the present work proposes two-dimensional definition of l_1 -norm minimization to an image matrix. A numerical experiment has been carried out to prove the capabilities and correctness of the image reconstruction algorithm. The analytical and experimental results show that the efficiency of the proposed algorithm, based on 2D l_1 -norm minimization depends on the sparsity of the observed surface. A small number of the dominated point scatterers from the surface guarantees better resolution in its final image.

Acknowledgment: This work is supported by the project of the National Science Fund T02/3, 2014.

References

1. Nicolas, J.-M., G. Vasile, M. Gay, F. Tupin, E. Trouvé. SAR Processing in the Temporal Domain: Application to Direct Interferogram Generation and Mountain Glacier Monitoring Can. – J. Remote Sensing, Vol. **33**, 2007, No 1, pp. 52-59.
2. Leijen, V., F. R. Hanssen. Interferometric Radar Meteorology: Resolving the Acquisition Ambiguity. – In: CEOS SAR Workshop, Ulm Germany, 27-28 May 2004, pp. 6-14.
3. Colesanti, C., A. Ferretti, F. Novali, C. Prati, F. Rocca. SAR Monitoring of Progressive and Seasonal Ground Deformation Using the Permanent Scatterers Technique. – IEEE Transactions on Geoscience and Remote Sensing, Vol. **41**, July 2003, No 7, pp. 1685-1701.

4. Figueiredo, M. A. T., R. D. Nowak, S. J. Wright. Gradient Projection for Sparse Reconstruction: Application to Compressed Sensing and Other Inverse Problems. – IEEE Journal of Selected Topics in Signal Processing, Vol. **1**, December 2007, No 4, pp. 586-597.
5. Tropp, J. Just Relax: Convex Programming Methods for Identifying Sparse Signals. – IEEE Transactions on Information Theory, Vol. **51**, 2006, pp. 1030-1051.
6. Kim, S.-J., K. Koh, M. Lustig, S. Boyd, D. Gorinevsky. An Interior-Point Method for Large-Scale l_1 -Regularized Least Squares. – IEEE Journal of Selected Topics in Signal Processing, Vol. **1**, 4 December 2007, pp. 606-617.
7. Donaho, D. L. Compressed Sensing. – IEEE Trans. on Inf. Theory, Vol. **52**, 2006, No 4, pp.1289-1306.
8. Hayashi, K., M. Nagahara, T. Tanaka. A User's Guide to Compressed Sensing for Communication Systems. – IEICE Trans. on Communications, Vol. **E96-B**, March 2013, No 3, pp. 685-712.
9. Gurbuza, A. C., J. H. McClellan, W. R. Scott, B. Jr. Compressive Sensing for Subsurface Imaging Using Ground Penetrating Radar. – Signal Processing, Vol. **89**, October 2009, No 10, pp. 1959-1972.
10. Cai, J.-L., C.-M. Tong, W.-J. Zhong, W.-J. Ji. 3D Imaging Method for Stepped Frequency Ground Penetrating Radar Based on Compressive Sensing. – Progress in Electromagnetics Research M, Vol. **23**, 2012, pp. 153-165.
11. McClellan, C. J. H., W. R. Scott. A Compressive Sensing Data Acquisition and Imaging Method for Stepped-Frequency GPRs. – IEEE Transation on Signal Processing, Vol. **57**, July 2009, No 7, pp. 2640-2650.
12. Shastry, M. C., R. M. Narayanan, M. Rangaswamy. Analysis of the Tolerance of Compressive Noise Radar Systems to Multiplicative Perturbations. – In: Proc. of SPIE'9109, Compressive Sensing III, 910905, 23 May 2014.
13. Lin, Y. G., B. C. Zhang, W. Hong, Y. R. Wu. Along-Track Interferometric SAR Imaging Based on Distributed Compressed Sensing. – Electronics Letters, Vol. **46**, 10 June 2010, No 12, p. 858-860.
14. Yang, J., J. Thompson, X. Huang, T. Jin. Random-Frequency SAR Imaging Based on Compressed Sensing. – IEEE Trans. on Geoscience and Remote Sensing, Vol. **51**, February 2013, No 2, pp. 983-994.
15. Li, J., S. Zhang, J. Chang. Applications of Compressed Sensing for Multiple Transmitters Multiple Azimuth Beams SAR Imaging. – Progress in Electromagnetics Research, Vol. **127**, 2012, pp. 259-275.
16. Wei, S.-J., X.-L. Zhang, J. Shi. Linear Array SAR Imaging Via Compressed Sensing. – Progress in Electromagnetics Research, Vol. **117**, 2011, pp. 299-319.
17. Wei, S.-J., X.-L. Zhang, J. Shi, G. Xiang. Sparse Reconstruction for SAR Imaging Based on Compressed Sensing. – Progress in Electromagnetics Research, Vol. **109**, 2010, pp. 63-81.
18. Qiu, W., E. Giusti, A. Bacci, M. Martorella, F. Berizzi et al. Compressive Sensing for Passive ISAR with DVB-T Signal. – In: Proc. of IRS-2013, 19-21 June 2013, pp. 113-118.
19. Kim, S., K. Koh, M. Lustig, S. Boyd, D. Gorinvesky. A Method for Large-Scale l_1 -Regularized Least Squares Problems with Applications in Signal Processing and Statistics. Tech. Report, Dept. of Electrical Engineering, Stanford University, 2007.
www.stanford.edu/~boyd/l1_ls.html